10/1/2021

Manuscript for Computers and Geotechnics

Title: Evaluating changes in the degree of saturation in excavation disturbed zones using a stochastic differential equation

Authors' names and affiliations:.

Yota Togashi[a,*], Kazuki Mizuo[b], Masahiko Osada[a], Tadashi Yamabe[c], and Hiroshi Kameya[d]

[a] *Graduate School of Science and Engineering, Saitama University 255 Shimo-Okubo Sakura, Saitama, Japan.* **E-mail**: togashi@mail.saitama-u.ac.jp, **Phone**: +81-48-858-3571, *Corresponding author

[b] *School of Civil Engineering, Saitama University (currently Staff Service Engineering Corporation), 255 Shimo-Okubo Sakura, Saitama, Japan.*

[c] *Crown Institute, 2-11-11 Kishi-cho Urawa, Saitama, Japan.*

[c] *OYO Corporation, 2-10-9 Daitakubo Minami, Saitama, Japan.*

Highlights:

1. Exact solution to the Richards' equation was derived for rock drying deformation.
2. Characteristics of the EDZ are modeled using Brownian motion.
3. A new stochastic differential equation is derived for water content changes in EDZs.
4. Validity of the proposed methods was confirmed using experimental data.

Abstract :

Deformation characteristics of sedimentary rocks significantly changed with the water content during drying. In tunnel construction, extremely small displacements such as geological disposal, are allowed. Therefore, the proper evaluation of such drying deformation phenomena is critical. In such scenarios, it is also essential to accurately assess water content changes in the rock masses. Furthermore, the excavation disturbed zone (EDZ) spreads around the tunnel owing to the excavation process. EDZ has a higher hydraulic conductivity than an intact rock mass. Therefore, it is essential to predict water content changes in EDZ within the scope of the drying deformation phenomena. In this study, we derived the exact solution to the Richards' equation at the Neumann boundary, which can be used to describe the drying phenomena in sedimentary rocks. Using japanese tuff, we conducted a permeability test and a mercury intrusion porosimetry test to obtain the water diffusion coefficient and verify whether their drying behavior can be described using the exact solution. Using the verified exact solution, we proposed a new stochastic differential equation that could be used to explain the local decrease in permeability and the increase in variations in EDZ, and applied the stochastic differential equation to 2D tunnel problem.

Keywords:

Richards' equation, excavation disturbed zone, moisture content, drying deformation

1. Introduction

Determining the deformation characteristics of sedimentary rocks during tunnel construction, considering small allowable displacements such as geological disposal, is essential. Specifically, the deformation characteristics of sedimentary rocks change significantly depending on their water content. Examining the drying deformation phenomena associated with the inflow of air during tunnel excavation is imperative (Osada, 2014). In a recent study, using tuff with deformation anisotropy, the authors established that the principal strain orientation rotated with changes in saturation, and the relatively stiff and soft directions reversed completely (Togashi et al., 2021a; Togashi et al., 2021b).Therefore, assessing the distribution of saturation to accurately predict the deformation of rock masses in tunnels is critical. Changes in the water content in a porous medium, including sedimentary rocks, follow the Richards' equation (Richards, 1931). Various analytical studies have been conducted based on the Richards' equation (Farthing and Ogden, 2017) to obtain exact solutions (Fleming et al., 1984; Ross and Parlange, 1994). Recently, various researchers have conducted studies in which they propose exact solutions by incorporating various nonlinear functions, such as the water diffusion coefficient, D (Abdoul et al., 2011; Hooshyar and Wang, 2016; Broadbridge et al., 2017). In some cases, the Boltzmann transformation was performed to convert the Richards' equation into a simple ordinary differential equation, after which it was solved (Zhou et al., 2013).

Although boundary conditions, such as Dirichlet boundary conditions, are often used to obtain the exact solution, Neumann boundary conditions are rarely utilized (e.g., Barry et al., 1993). With regards to drying deformation phenomena, sudden changes in the water content of rock masses that are in contact with the atmosphere do not occur. Therefore, it is vital to define a Neumann boundary. During tunnel excavation, the surrounding rock mass becomes loose, and the excavation disturbed zone (EDZ) expands. Therefore, it is crucial to evaluate the EDZ while examining the drying deformation phenomena. Previous studies have shown that the permeability of the EDZ increases as the distance to the well wall decreases (Hou, 2003; Marschall et al., 2016; Lisjak et al., 2016). Other researchers have compared and modeled the water diffusion coefficients of the EDZ and intact rocks (Autio et al., 1998). Similarly, the permeability of the EDZ has been analyzed. However, there is no unified view because its properties differ with the location characteristics, such as the geological conditions and the surface stress fields. Specifically, the obtained permeability varies widely because the excavation disturbance is contiguous with the tunnel wall (Kurikami et al., 2008).

Therefore, we derived the exact solution to the Richards' equation using the Neumann boundary in this study, which can be used to describe the drying phenomena in sedimentary rocks. Using tuff samples collected in Japan, we conducted a hydraulic conductivity test and a mercury intrusion test via the flow pump method to obtain the water diffusion coefficients and verify whether the drying behavior can be described using the exact solution. Using the verified exact solution, we proposed a new stochastic differential equation that can be used to express the local variations in permeability as well as the increase in variations.

2. Numerical method for determining the distribution of the degree of saturation in the EDZ owing to drying

2.1 Exact solution to Richards' equation considering Neumann boundary conditions for drying phenomena

We proposed the following nonlinear partial differential equation to predict changes in the water content of unsaturated ground (Richards, 1931):

$$\frac{\partial \theta}{\partial t} = \frac{\partial K}{\partial r}\left(\frac{\partial \psi}{\partial r} + 1\right), \tag{1}$$

where θ, t, K, r, and ψ represent the volumetric water content, time, unsaturated hydraulic conductivity, coordinate, and pressure head, respectively. The exact solution to this nonlinear partial differential equation remains unknown. However, in this study, we obtained the exact solution to this equation using a method that is similar to that employed in a previous study conducted by Barry et al. (1993). Because this method was significantly simplified, its derivation is described in detail below. The Richards' equation was transformed into the following:

$$\frac{\partial \theta}{\partial t} = \frac{\partial}{\partial r}\left(K \frac{\partial \psi}{\partial \theta}\frac{\partial \theta}{\partial r}\right) + \frac{\partial K}{\partial r}, \tag{2}$$

where the heat equation can be obtained by considering that the water diffusion coefficient, D, which is the slope of the water retention curve, is always a constant ($D = K\partial\psi/(\partial\theta) = \text{const.}$) (Gardner, 1958). Furthermore, we also considered that the unsaturated hydraulic conductivity does not depend on the coordinates ($\partial K/(\partial r) = 0$).

$$\frac{\partial \theta}{\partial t} = D\frac{\partial^2 \theta}{\partial r^2}. \tag{3}$$

The water retention curve is predominantly nonlinear in the region adjacent to saturation and dryness. However, the assumption that the value of D is constant in the region where S is neither too small nor too large holds. It is also rational to assume that K does not depend on coordinates, if the stratum is uniform. The following can be obtained by substituting the effective saturation $S = (\theta - \theta_r)/(\theta_s - \theta_r)$ into the equation presented above using the volume moisture content, θ_s, at saturation and the residual volume moisture content, θ_r (Tracy, 2011):

$$\frac{\partial S}{\partial t} = D\frac{\partial^2 S}{\partial r^2}. \tag{4}$$

Further, we set the initial and boundary conditions. First, the following equation was assumed as the initial condition:

$$S(r, 0) = S_i. \tag{5}$$

We considered a closed interval, where r is $[0, L]$, and S_i is a constant value. Here, the following Neumann boundary conditions were introduced to manage the various boundary conditions (Farlow, 1993):

$$\frac{\partial S(0,t)}{\partial r} = 0, \quad -\frac{\partial S(\pm L, t)}{\partial r} = h(S - S_t), \tag{6}$$

where S_t represents the constant terminal saturation value. Although 0 to L for the interval of r was used in this study, the exact solution was derived from $-L$ to L to obtain the requisite boundary conditions. The result is shown using $0 \leq r \leq L$. Because the exact solution cannot be obtained as is, we introduced the dimensionless saturation degree, $s_d(r,t) = (S(r,t) - S_t)/(S_i - S_t)$, and we modified the equation as follows:

$$\frac{\partial s_d}{\partial t} = D\frac{\partial^2 s_d}{\partial r^2}, \tag{7}$$

$$s_d(r, 0) = \frac{S(r,t) - S_t}{S_i - S_t} = 1, \tag{8}$$

and

$$\frac{\partial s_d(0,t)}{\partial r} = 0, \quad -\frac{\partial s_d(\pm L,t)}{\partial r} = h s_d. \tag{9}$$

First, the general solution to Eq. (7) can be expressed as follows:

$$s_d = \left(A \cos pr + B \sin pr\right) C e^{-Dp^2 t}, \tag{10}$$

where A, B, and C represent undetermined coefficients, and p represents a nonzero positive real number. By differentiating this equation with r and substituting $r = 0$, the following equation was obtained using the boundary conditions used in Eq. (9):

$$\left(-Ap \sin pr + Bp \cos pr\right) C e^{-Dp^2 t} \mid_{r=0} = BpCe^{-Dp^2 t} = 0. \tag{11}$$

When the value of C is zero, the value of s_d is always zero, and thus, $B = 0$. Similarly, by substituting the boundary condition of $r = L$ in Eq. (9), we obtained the following:

$$-\left(-Ap \sin pr\right) C e^{-Dp^2 t} \mid_{r=L} = Ap(\sin pL)Ce^{-Dp^2 t} = hA(\cos pL)Ce^{-Dp^2 t}. \tag{12}$$

Therefore, we obtained the following relational expression for p:

$$p \tan pL = h. \tag{13}$$

If the solutions that satisfy Eq. (13) are $p_1,\ p_2,\ p_3 \cdots$, then their linear sum is also a solution. Therefore, s_d can be expressed as follows:

$$s_d = \sum_{n=1}^{\infty} \left(C_n \cos p_n r\right) e^{-Dp_n^2 t}. \tag{14}$$

Substituting the initial condition used in Eq. (8) into this equation yielded the following:

$$s_d(r,0) = 1 = \sum_{n=1}^{\infty} \left(C_n \cos p_n r\right). \tag{15}$$

To determine the Fourier coefficient, C_n, the right-hand sides of the equations mentioned above for n and $\cos p_m,\ (m = 1, 2, \cdots)$ were multiplied and integrated. This integral has a value only when

$m = n$ owing to the orthogonality of the trigonometric function, as shown below:

$$\int_0^L C_n \cos p_n r \cdot \cos p_m r dz = C_n \left(\frac{\sin(2p_n L)}{4p_n} + \frac{L}{2} \right). \tag{16}$$

Therefore, this equation is equal to the following equation:

$$\int_0^L 1 \cdot \cos p_m r dz = \frac{\sin(p_m L)}{p_m}. \tag{17}$$

From the equations presented above, C_n can be obtained as follows:

$$C_n = \frac{4 \sin(p_n L)}{\sin(2p_n L) + 2p_n L}. \tag{18}$$

Therefore, the exact solution to s_d is expressed as follows:

$$s_d = \sum_{n=1}^{\infty} \frac{4 \sin(p_n L)}{\sin(2p_n L) + 2p_n L} (\cos p_n r) e^{-Dp_n^2 t}. \tag{19}$$

When the change in the variables used in Eq. (8) is taken back, an exact solution for the degree of saturation, S, can be obtained by setting $\beta_n = p_n L$, as follows:

$$S(r,t) = S_t + (S_i - S_t) \sum_{n=1}^{\infty} \frac{4 \sin(\beta_n)}{\sin(2\beta_n) + 2\beta_n} (\cos \beta_n r/L) e^{-D\beta_n^2 t/L^2}. \tag{20}$$

As shown in Eq. 13, β_n is the solution to the following transcendental function, which was solved using the Newton–Raphson method:

$$\frac{\beta_n}{Lh} = \cot \beta_n \tag{21}$$

2.2 Stochastic differential equation for describing the distribution of the degree of saturation in the EDZ owing to drying

Unpredictable random behavior is known as Brownian motion, which is named after Dr. R. Brown who discovered that pollen particles floating on the surface of water move irregularly. The total derivative first-order differential equation that includes Brownian motion is referred to as a stochastic differential equation in the field of financial engineering. It is used to predict and set stock prices for financial products. Because ordinary Brownian motion is used to describe future uncertainties, it is a random motion that accumulates one variance of time per unit of time. In a homogeneous stratum, the nature of the EDZ is such that the vicinity of the excavated tunnel wall gets disturbed and develops cracks, resulting in heterogeneous and random properties. However, areas farther from the tunnel wall have more homogeneous properties. This can be explained by the Brownian motion of the variable, r, because the larger the value of r (Fig. 1), the more the variance accumulates and demonstrates random properties. In this study, we proposed a stochastic

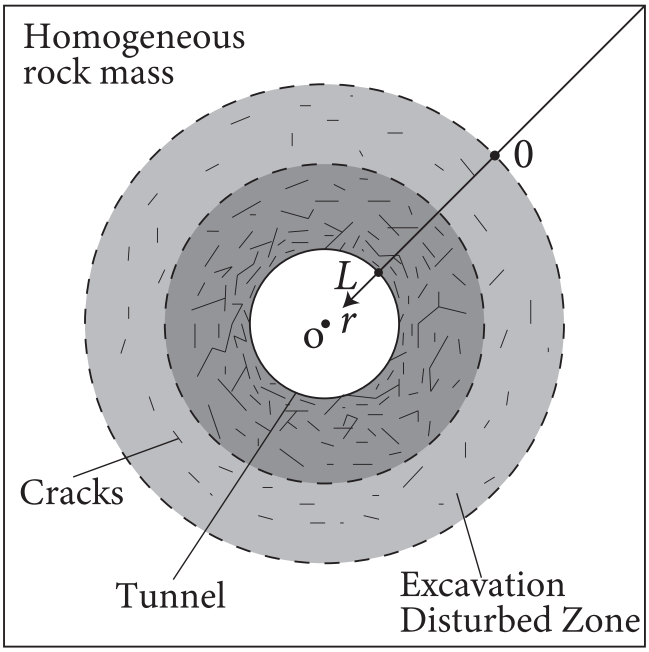

Fig.1 Concept of the excavation disturbed zone (EDZ). r represents the coordinates towards the center of the tunnel, and L represents the width of the EDZ. Random characteristics increase as the values of the coordinate r increase.

differential equation that estimates the distribution of the saturation degree in the EDZ by utilizing the following characteristics:

$$dS^*(r,t) = dS(r,t)\left(1 + \sigma dW(r)\right), \tag{22}$$

where S^*, S, σ, and W represent the distribution of saturation based on the properties of the EDZ, exact solution to Eq. (20), volatility that controls the magnitude of Brownian motion, and Wiener process indicating Brownian motion, respectively. Because the infinitesimal increment in the exact solution (Eq. (20)) is the coefficient of the term that includes Brownian motion, S^* always converges to S_t by $t \to \infty$, regardless of the magnitude of σ. Figure 2 shows an example of Brownian motion, W, generated under this condition. Thus, the random property increases with an increase in the variable, i.e., r. The increase in permeability variation in the EDZ (Kurikami et al., 2008) has been investigate. However, the properties of the EDZ have not been expressed using Brownian motion.

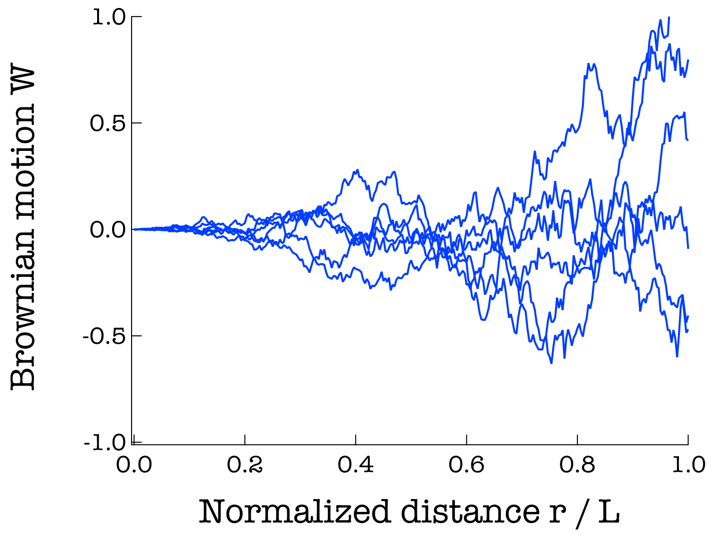

Fig.2 Relationship between random EDZ characteristics using Brownian motion and distance r. It can be determined that the closer r is to L, the more random the property is, as shown in Fig. 1.

3. Detection of hydraulic conductivity and water retention characteristics

In this study, the moisture diffusion coefficient, D, was assumed to be constant. $S = (\theta - \theta_r)/(\theta_s - \theta_r)$. If θ is differentiated using S, then $\frac{dS}{d\theta} = \frac{1}{\theta_s - \theta_r}$ can be obtained. Therefore, the expansion of the formula for D is expressed as follows:

$$
\begin{aligned}
D = K\frac{\partial\psi}{\partial\theta} &= K\frac{\partial\psi}{\partial S}\frac{\partial S}{\partial\theta} \\
&= K\cdot\frac{\partial\psi}{\partial S}\cdot\frac{1}{\theta_s-\theta_r},
\end{aligned}
\tag{23}
$$

where K represents the unsaturated hydraulic conductivity. If the saturated hydraulic conductivity, k_s, is proportional to the degree of saturation, the unsaturated hydraulic conductivity can be described as $K = k_sS$. Therefore, K can be determined from the saturated hydraulic conductivity test. In the equation presented above, the values of θ_s and θ_r were determined using a mercury intrusion porosimetry test because the void volume in the sample can be determined using this test. $\frac{\partial\psi}{\partial S}$ represents the slope of the water retention curve, which can be obtained by performing a mercury intrusion porosimetry test for rocks. The following sections detail the three tests conducted in this study to obtain D.

3.1 Rock sample

A Neogene tuff collected from a depth of 100 m in Utsunomiya City, Japan, was used as the rock test sample. This marine-origin tuff was formed by the consolidation of eruptive deposits that originated from submarine volcanoes dated to 10 Mya. This green tuff is known as a Tage tuff, as shown in Fig. 3. It is widely used in Japan as a research sample and building material (e.g., the old Imperial Hotel in Japan designed by Frank Lloyd Wright). This tuff has uniform and homogeneous properties. The minerals contained in the Tage tuff are tuffy glass, plagioclase, quartz, and biotite amphibole pyroxene (Seiki, 2017). The physical properties of the Tage tuff are listed in Table 1. Tage tuff is characterized by a large porosity and a slightly soft deformation property (Togashi et

Table 1 Physical properties of the Tage tuff

Density in natural state ρ_t(Mg/m^3)	Dry density ρ_d(Mg/m^3)	Wet density ρ_t(Mg/m^3)	Porosity %	Natural moisture content ratio w (%)
1.81	1.76	2.04	26.7	3.8

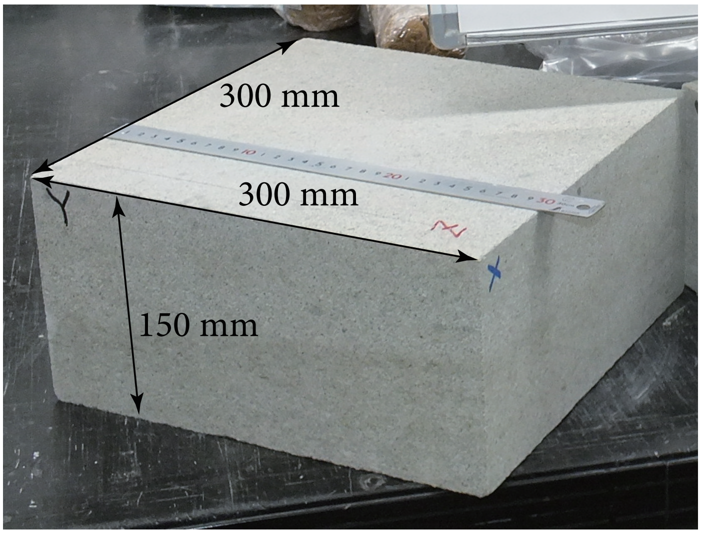

Fig.3 Cuboidal block sample of Tage tuff.

al., 2018; Togashi et al., 2019; Togashi et al., 2021c). The porosity of the sample was determined using the soil particle density test, which yielded a density of 2.56 Mg/m^3.

3.2 Permeability test

The hydraulic conductivity was obtained using the flow pump method (Esaki et al., 1996), where the saturated hydraulic conductivity is obtained by controlling the flow rate using a syringe pump, as shown in Fig. 4, and measuring the pressure head difference. Saturated hydraulic conductivity can be expressed as follows:

$$k_s = \frac{Q}{At}\frac{H}{\psi}, \tag{24}$$

where Q, A, t, and H represent controlled flow rate, cross-sectional area of the specimen, time, and length of the specimen, respectively. The room temperature was maintained at 22 °C.

3.3 Mercury intrusion porosimetry test

In the mercury intrusion porosimetry test, mercury is press-fitted while pressurizing a dry sample, and the distribution of the gap diameter in the sample is inferred based on the pressure and the

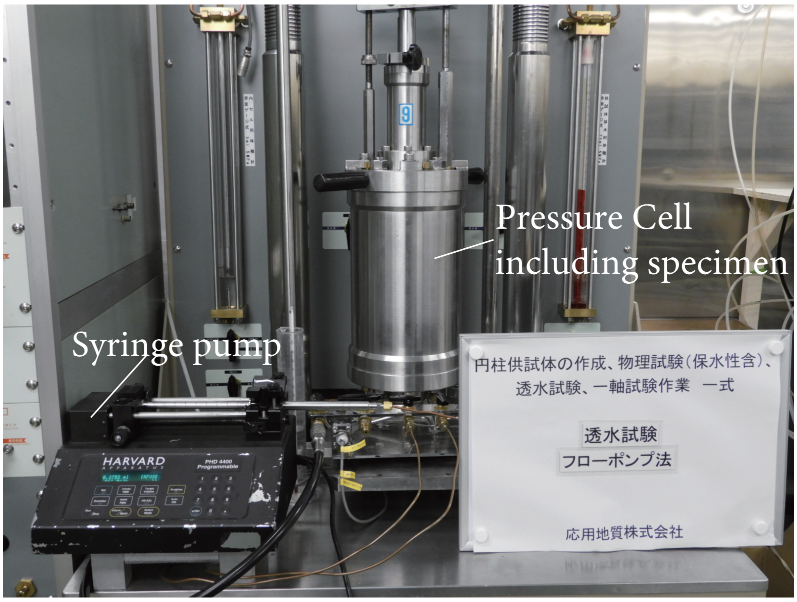

Fig.4 Permeability test based on the flow pump method

amount of press-fitted mercury (Thomas et al., 1968; ASTM, 2004). This test is used to determine the void diameter distribution of a sample. However, in this study, it was used to determine the water retention curve, as proposed in previous studies (Sun and Cui, 2020). From the results of this test, the degree of saturation, S, was calculated as follows:

$$S = \frac{CI(P)}{CI(P_{max})}, \tag{25}$$

where CI represents the amount of press-fitted mercury, P represents the arbitrary press-fitting pressure, and P_{max} represents the maximum pressure. By investigating S using P as the capillary pressure, a water retention curve could be obtained.

3.4 Detection of continuous moisture content variation using the drying deformation test

Figure 5 shows the drying deformation experiment (Togashi et al., 2021a). In this experiment, a strain gauge was installed on a wet rock specimen, which was air dried. The change in the water content was measured using an electronic balance. We estimated the change in saturation by considering the change in the void structure estimated from the deformation of the specimen. The cylindrical Tage tuff specimen, with a diameter of 50 mm and a height of 100 mm, had a volumetric strain of approximately 2,000 μ with changes in its void diameter. The degree of saturation was estimated considering the change in void diameter owing to drying (Togashi et al., 2021a). Using the time-series changes in the saturation of the Tage tuff measured using this method, the validity of the exact solution to the Richards' equation, as derived previously, was verified.

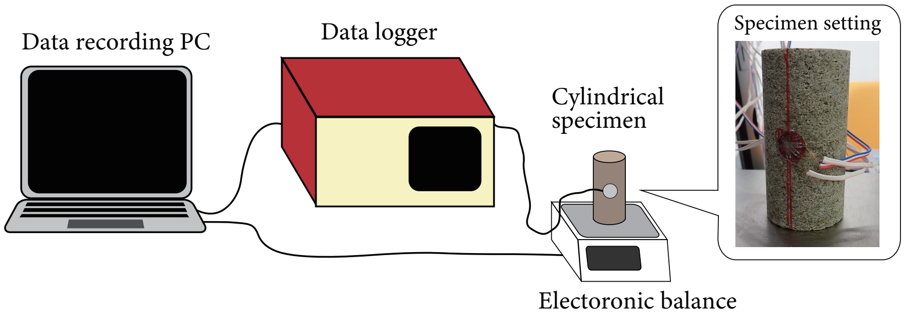

Fig.5 Drying deformation experiment (Togashi et al., 2021a).

4. Verification of the exact solution to the Richards' equation

4.1 Identifying parameters that compose D

The results obtained from the permeability and mercury intrusion porosimetry tests are listed in Table 2. The obtained saturated permeability coefficient, k_s, was the average value obtained from nine specimens. However, the permeability coefficient was rather small for its correspondingly large porosity. Similar findings have also been reported in previous studies (Watanabe and Sato, 1979). Therefore, the value obtained for hydraulic conductivity was considered appropriate. The void volume could be obtained from the volume of the press-fitted mercury in the mercury intrusion porosimetry test. The void volume obtained was the average value of three mercury intrusion tests. Volume moisture content can be defined as θ and $\theta = \frac{V_w}{V}$, where V_w and V represent the water volume and total volume, respectively. Because the volume of the void is equal to the water volume, V_w, at saturation, the total volume, V, was calculated using the mass and dry density, ρ_s, of the sample in the mercury intrusion test. Finally, the saturated volume moisture content was determined. Thus, the value of $\frac{1}{\theta_s-\theta_r}$ was 3.8, assuming that $\theta_r = 0$.

Table 2 Results of the permeability test and the mercury intrusion porosimetry test

Saturated hydraulic conductivity k_s (m/s)	Void Volume (cm^3/g)	Saturated volume moisture content Moisture content θ_s
5.7×10^{-11}	0.15	0.26

Figure 6 shows the water retention curve obtained using Eq. (25) in the mercury intrusion test. A value of $P = 5$ MPa, which is equivalent to the suction specified at $S = 0.13$, was confirmed in the dry deformation experiment conducted in a previous study (Togashi et al., 2021a), thereby validating this result. As shown in Fig. 6, the inclination of the curve was relatively constant from $S = 0.2 - 0.9$. Therefore, the value of $\frac{\partial \psi}{\partial S}$ corresponds to 341.4 m as the suction is converted to a pressure head of $\psi = P/(\rho_w g)$, where ρ_w $(= 1.0(\mathrm{g/cm^3}))$ and g $(= 9.81\mathrm{m/s^2})$ represent the water density and gravitational acceleration, respectively. The unsaturated hydraulic conductivity,

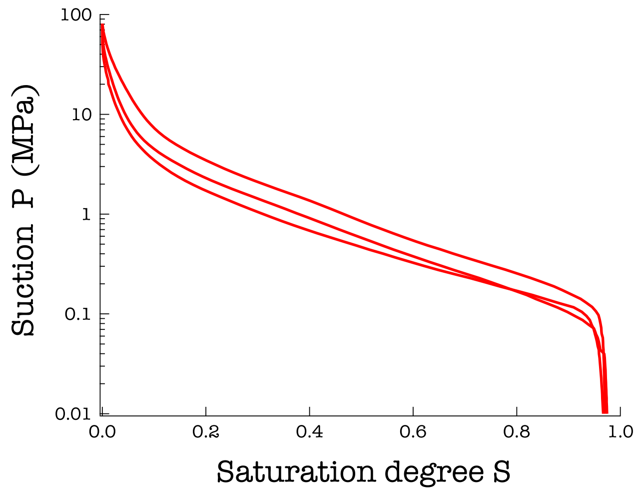

Fig.6 Water retention curve (relationship between suction P and degree of saturation S) for the Tage tuff.

$K = Sk_s = 0.55 \times 5.7 \times 10^{-11} = 3.1 \times 10^{-11}$ when calculated in the middle of $S = 0.9 - 0.2$. Therefore, the desired value of D can be calculated as follows: $D = K \cdot \frac{\partial \psi}{\partial S} \cdot \frac{1}{\theta_s-\theta_r} = 3.1 \times 10^{-11} \cdot 341.4 \cdot 3.8 =$

4.02×10^{-8} (m^2/s). Corresponding to calculation of the drying process of $S = 0.9$ to 0.2, $\frac{\partial \psi}{\partial S}$ was set as positive in the direction of increasing suction, which is opposite to that illustrated in Fig. 6.

4.2 Nature of the exact solution

Using the value of D specified in the previous section, we assessed the nature of the exact solution (Eq.20). Figure 7 shows the effect of the difference in the value of h on the exact solution. The input parameters of the exact solution are listed in Table 3. Here, $L = 0.1$ m was set to accelerate

Table 3 Input parameters of the exact solution.

Initial saturation degree S_i	Terminal saturation degree S_t	D (m^2/s)	L (m)	Number of Fourier series terms n
0.9	0	4.02×10^{-8}	0.1	100

the convergence of the degree of saturation, and S_i and S_t were set to 0.9 and 0, respectively. To observe the nature of the solution over a wide area, we performed calculations in which the value of S ranged from 0.2–0.9 by assuming linearity based on the previous section. The results are presented as the distribution of the daily values of r for 20 d. The number of terms, n, in the Fourier series for the exact solution was set to 100. Larger values of h yielded an enhanced convergence of the degree of saturation based on its closeness to the Dirichlet boundary condition. Additionally, the smaller the value of h, the closer the degree of saturation is to a constant inside the region. Introducing the Neumann boundary condition allowed various geological situations to be expressed.

4.3 Comparison between the exact solution and test results for verification

Figure 8 shows a comparison of the exact solution proposed and the results obtained through the dry deformation experiment. In the experiment, the cylindrical specimen was soaked in water for ≥ 10 d to increase the degree of saturation to approximately 0.8, after which air drying was performed. The input parameters of the exact solution are listed in Table 4. Here, the exact solution

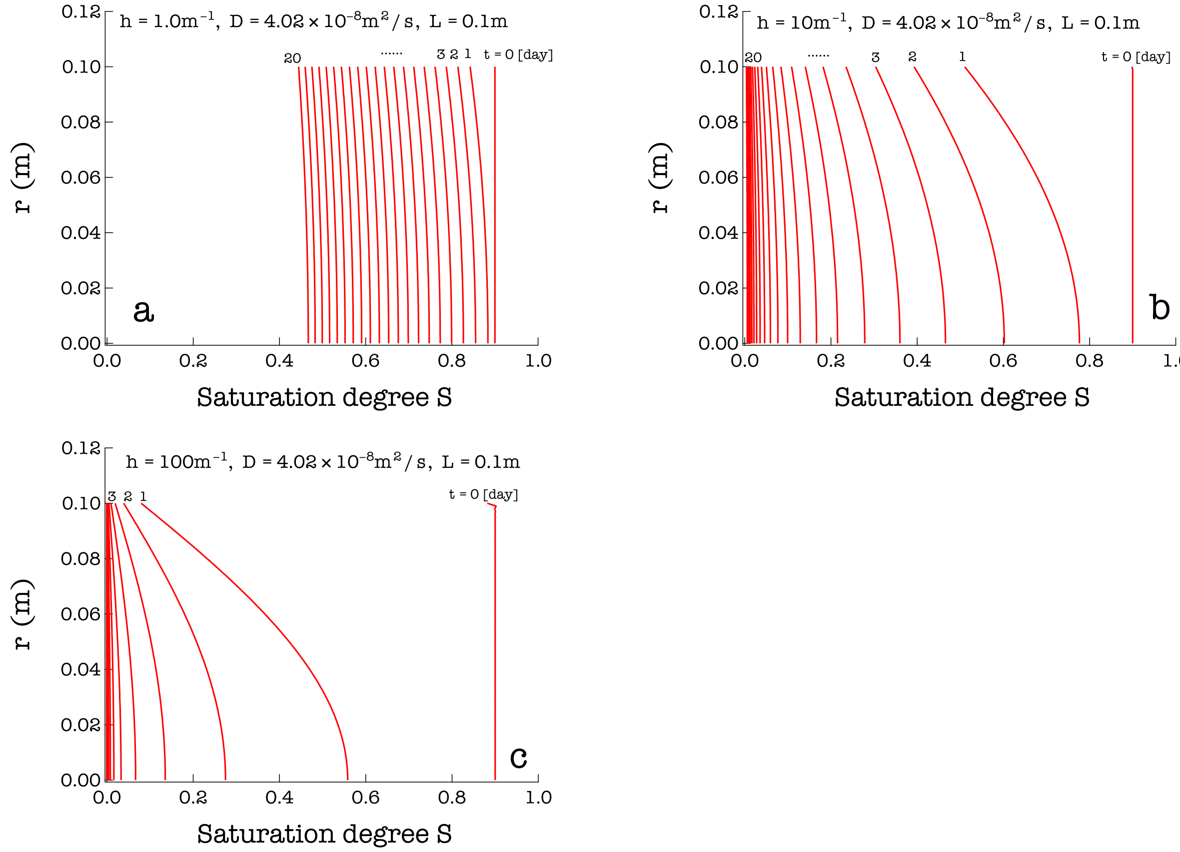

Fig.7 Characteristics of the exact solution (degree of saturation S and its relationship to distance r) based on $D = 4.02 \times 10^{-8}$ (m^2/s): (a) $h = 1$ m^{-1}, (b) $h = 10$ m^{-1}, and (c) $h = 100$ m^{-1}.

Table 4 Input parameters of the exact solution.

Initial saturation degree S_i	Terminal saturation degree S_t	D (m^2/s)	h (m^{-1})	L (m)	Number of Fourier Series terms n
0.81	0	4.02 $\times 10^{-8}$	12.2	0.0375	100

was calculated using the value of D obtained in Section 4.1. The values of S_i and S_t were set to 0.9 and 0, respectively. The exact solution exceeded the linearity range of the water retention curve assumed in the range of $S = 0.2 - 0.9$ when the value of D was calculated in the previous section. However, we rectified the error. The data for the exact solution showed a change in the degree of saturation at $x = 0$, where the value of h was set to 12.2 m^{-1}. In the experiment, the length of the region was L = 0.0375m, average value of the half diameter was 25 mm, and half height was 50 mm for the cylindrical specimen. Here, the value of L was set by assuming an element test to examine uniform behavior. However, if the value of L was on the same level, it could be adjusted by changing the value of h. The results were in good agreement, even in the region where the value of S was small. Because the experimental values and the exact solution were nearly identical, we confirmed the validity of our proposed exact solution.

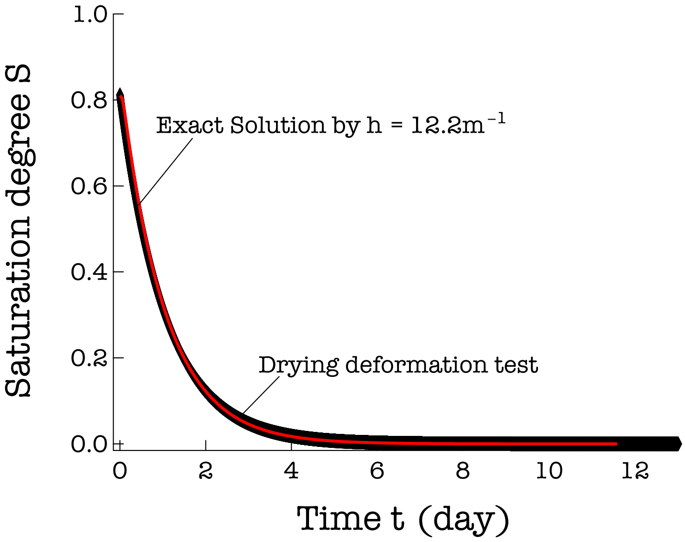

Fig.8 Comparison of the degree of saturation S and time t relationships between the exact solution and the results of the drying deformation test.

5. Random distribution of the degree of saturation in the EDZ

In this section, we discuss the properties of the stochastic differential equation presented in Eq. (22) using the exact solution. Equation (22) was solved using the Euler–Maruyama method (Higham, 2001). This is a type of backward finite differential method, which can be derived as follows: For the region of $[0, L]$, let $\Delta r = r/N$ be an infinitesimal increment in the coordinate direction r. Here, N represents the number of divisions in the area. Using the positive integer j, r_j can be expressed as follows: $r_j = j\Delta r$. Therefore, Eq. (22) can be further modified as follows:

$$\begin{aligned} dS^* &= dS\,(1 + \sigma dW) \\ &= \frac{\partial S}{\partial r} dr\,(1 + \sigma dW)\,. \end{aligned} \tag{26}$$

When the Euler-Maruyama method was applied with dr as Δr, the following backward differential equation was obtained:

$$S^*(r_j,t) = S^*(r_{j-1},t) + \frac{\partial S}{\partial r}(r_{j-1},t)\Delta r\left[1+\sigma\left(W(r_j)-W(r_{j-1})\right)\right]. \tag{27}$$

The relationship between W_j and W_{j-1} can be expressed as follows (Higham, 2001):

$$\begin{aligned} W_j &= W_{j-1} + dW_j \\ &= W_{j-1} + \sqrt{\Delta r}N(0,r), \end{aligned} \tag{28}$$

where $N(m,\Sigma)$ represents a normal random number with a mean of m and a variance of Σ. The properties and applications of Eq. (22), as obtained through this method, are discussed in the following section.

5.1 Nature of the proposed stochastic differential equation

Figure 9 shows the solution of the proposed stochastic differential equation when $\sigma = 0$ and 100. When $\sigma = 0$, the random term W is not included in the equation, and thus, it is identical to the solution for Eq. (20). The input parameters of the exact solution are listed in Table 5. To set

Table 5 Input parameters of the proposed stochastic differential equation.

Initial Saturation degree S_i	Terminal saturation degree S_t	D ($\mathrm{m^2/s}$)	h ($\mathrm{m^{-1}}$)	L (m)	Number of Fourier Series terms n	N
0.81	0	4.02×10^{-8}	12.2	1.0	100	300

the values of D, h, S_i, and S_t, we used the parameters of the Tage tuff determined in the previous section. The values of L and N were set to 1 m and 300, respectively. Figure 9 shows the results at different times, i.e., $t = 0$, 50, 100, and 1000 d. Even when the value of the random term σ was large, the exact solution reached a constant value, S_t, as t elapsed. To determine the difference in σ, solutions containing random terms with $\sigma = 20$ were distributed along the exact solution for Eq. (20) with $\sigma = 0$. As the value of z increased, there was an increase in the uncertainty of the Brownian motion, and as such, there was an increase in the influence of the random term. The

Brownian motion according to coordinate r was generated using the same normal random number with a mean of 0 and a variance of r because the nature of the EDZ was assumed to be invariant with respect to time. Therefore, relatively similar noise was generated in the results pertaining similar values of r, and this saturation distribution reflects the properties of the EDZ.

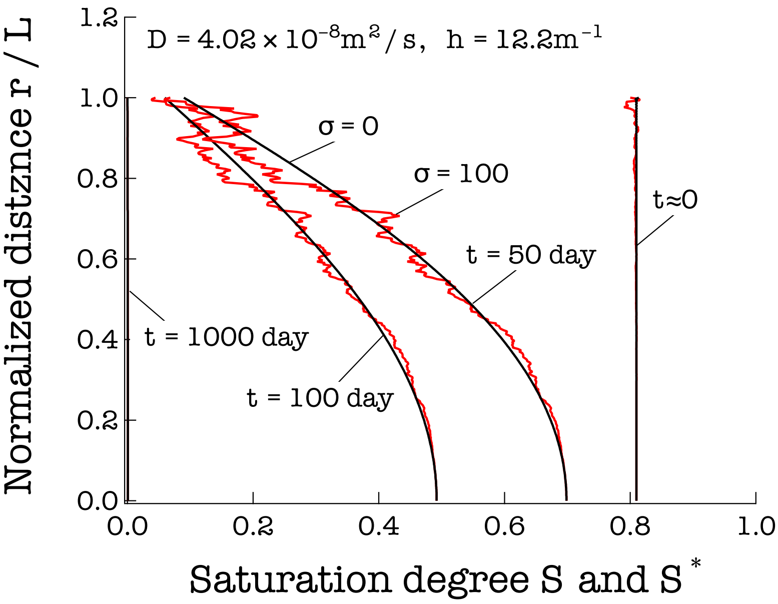

Fig.9 Distributions of the degree of saturation at distance r owing to the volatility of σ and time t for the EDZ and its characteristics.

As shown in Figure 10, $t = 100$ d and $\sigma = 100$. The effect of N was investigated using parameter settings similar to those presented in Fig. 9. When the value of N is insignificant, the difference step is large, and as a result, the effect of the random term is significant. As shown in the example presented in Fig. 10 ($N = 50$), the value of S is ≥ 1, which is unrealistic. Additionally, when the value of N is insignificant, the effect of the random term is negligible. Because the value of N also affects the level of uncertainty, a realistic value must be set. Considering this parameter setting, $N > 100$ would be preferable.

As described above, our proposed stochastic differential equation can be used to express the properties of the EDZ, and the influence of the random terms can be determined using σ and N.

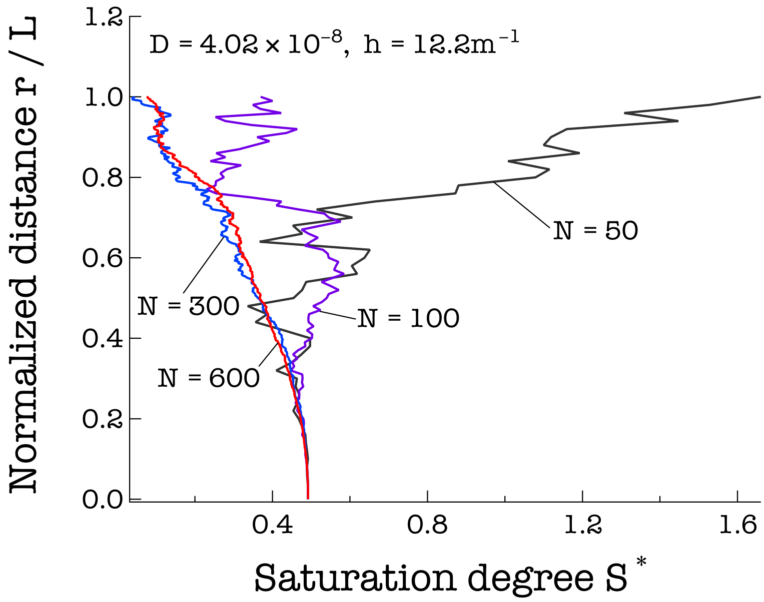

Fig.10 Effect of N on random terms for the distribution of the degree of saturation at distance r

5.2 Method verification

Differences in the saturated hydraulic conductivity at approximately 1–10 m behind the tunnel wall have been investigated by conducting laboratory tests using a boring core or through in situ hydraulic conductivity tests (Hou, 2003; Marschall et al., 2006; Kurikami et al., 2008). In these studies, the hydraulic conductivity varied from 10^4 to 10^{10} m/s at the maximum as it approached the well wall. Specifically, the sedimentary rock sites targeted in this study have a maximum variation of 10^4 m/s (Kurikami et al., 2008).

In this study, we considered a case in which the saturated hydraulic conductivity, k_s, of the intact Tage tuff was disturbed by tunnel excavation, and it increased by 10^4 m/s. Meanwhile, if the hydraulic conductivity of the intact part ($r = 0$) and that of the disturbed part ($r = L$) are linearly interpolated in the rock mass, the intermediate average hydraulic conductivity, k_s, is 5.7×10^{-11} m/s.

As shown in Fig. 11, the validity of the proposed method was evaluated by solving the stochastic differential equation presented in Eq. (22) using the average hydraulic conductivity, with $\sigma = 20$, and comparing it with the results of the hydraulic conductivity of the intact and disturbed parts, with $\sigma = 0$. This comparative analysis approach relied on the data listed in Table 5, except for D. Each value of D was calculated using $k_s = 5.7 \times 10^{-11}$ m/s for the intact part and $k_s = 5.7 \times 10^{-7}$ for the disturbed part. $k_s = 5.7 \times 10^{-9}$ m/s was employed in the average case using the stochastic differential equation [Eq. (22)]. Equation (22) was solved 100 times using different Brownian motions, W. Figure 11 shows the results 10 d after the experiment, at which point the disturbed rock

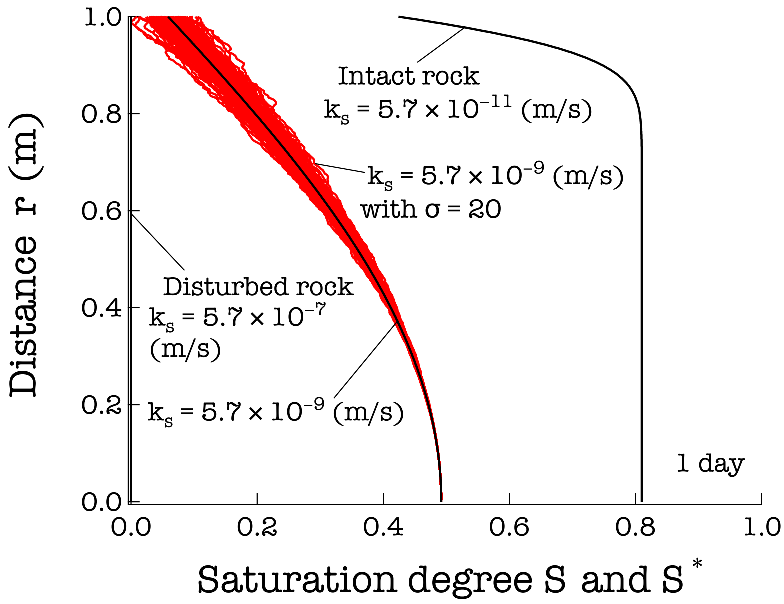

Fig.11 Comparison between the proposed stochastic differential equations using the average hydraulic conductivity and the distribution of the saturation degree in the intact and disturbed parts.

mass had already converged, where $S = 0.42$ at $r = L$. For the stochastic differential equations, the average hydraulic conductivity lies between the results of the intact case and those of the disturbed case. Although the hydraulic conductivity was distributed across the actual rock mass, the hydraulic conductivity was insignificant in the disturbed part near the tunnel wall. Therefore, the behavior near the tunnel wall was similar to that of the disturbed case.

As the degree of saturation in the part with high hydraulic conductivity near the mine wall decreases, there is a corresponding decrease in the degree of saturation in the intact part. Therefore, the degree of saturation near $r = 0$ was considered smaller than that in the case involving hydraulic conductivity in the intact part. Furthermore, presuming that the hydraulic conductivity in the EDZ has a large variation, we can conclude that the results of the stochastic differential equation [Eq. (22)] are generally rational.

5.3 Random distribution of the degree of saturation around a circular tunnel owing to drying

Assuming that the drying phenomena occurs uniformly around the tunnel owing to tunnel excavation without considering groundwater advection, we can estimate the distribution of the degree of saturation around the tunnel using the 1D stochastic differential equations proposed in this study. For example, this condition is applicable when constructing a deep tunnel, such as in geological disposal, because it can be assumed that the head difference between the tunnel crown and the invert is small from a macroscopic perspective. Considering the analysis area presented in Fig. 12, we assumed that the 1D equation [Eq. (22)] can be applied in the r axis orientation in each circumferential direction, Θ.

Figure 13 presents a comparison of this analysis approach when $\sigma = 0$ and $\sigma = 30$. Here, using the Igor Pro graphing software, the 3D coordinate points were contoured under the same conditions. The set analysis conditions were similar to those listed in Table 5, differing by only $N = 300$ after 100 d of excavation. As drying progressed from the wall surface of the tunnel, this part had the lowest saturation. The result of $\sigma = 0$ assumes that cracks do not occur during excavation. Furthermore, a smooth curved surface with a distributed degree of saturation can be confirmed. In contrast, for $\sigma = 30$, the variation in saturation increased as it approached the surface of the tunnel wall.

Moreover, for $\sigma = 30$, which considers the formation of the EDZ owing to excavation, the variation in saturation increased as it approached the surface of the tunnel wall, unlike in the EDZ shown in Fig. 1.

Furthermore, utilizing this analysis method, we can consider the anisotropy of the spatial variation

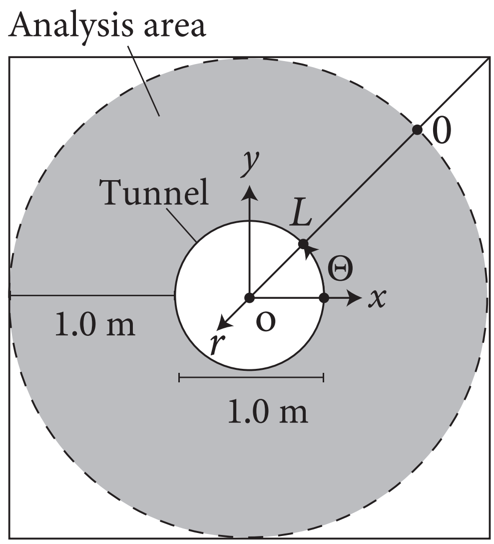

Fig.12 Analytical area of the EDZ. r represents a coordinate system that radiates towards the center of the tunnel. $(x,\ y)$ represents a two-dimensional Cartesian coordinate system. Θ represents the angle between the x and r axes.

in the saturation. The following function distributes σ in the circumferential direction, Θ:

$$\sigma = p|\sin\Theta| + q, \tag{29}$$

where p and q represent appropriate real numbers. Figure 14 shows the results of the same analysis performed at $p = 150$ and $q = 30$. This indicates that the variation in the saturation on the y axis is five-fold larger than that on the x axis. Sharp irregularities accumulate on the y axis (x axis), which is possible if the crustal pressure is anisotropic.

6. Conclusions

Evaluations of the water content in EDZs are indispensable for proper assessments of the deformation characteristics of the rock mass around a tunnel. In this study, we derived a simple exact solution to the Richards' equation considering the Neumann boundary for drying deformation phenomena. We performed permeability and mercury intrusion porosimetry tests on Neogene tuff obtained from Japan, and the water diffusion coefficient was specified based on the obtained

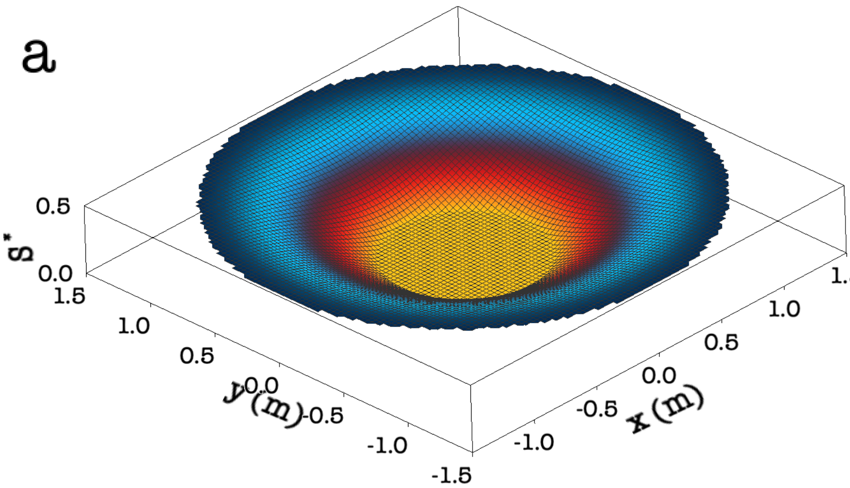

Fig.13 Comparison of the distribution of the degree of saturation around the tunnel owing to drying: (a) $\sigma = 0$ and (b) $\sigma = 30$.

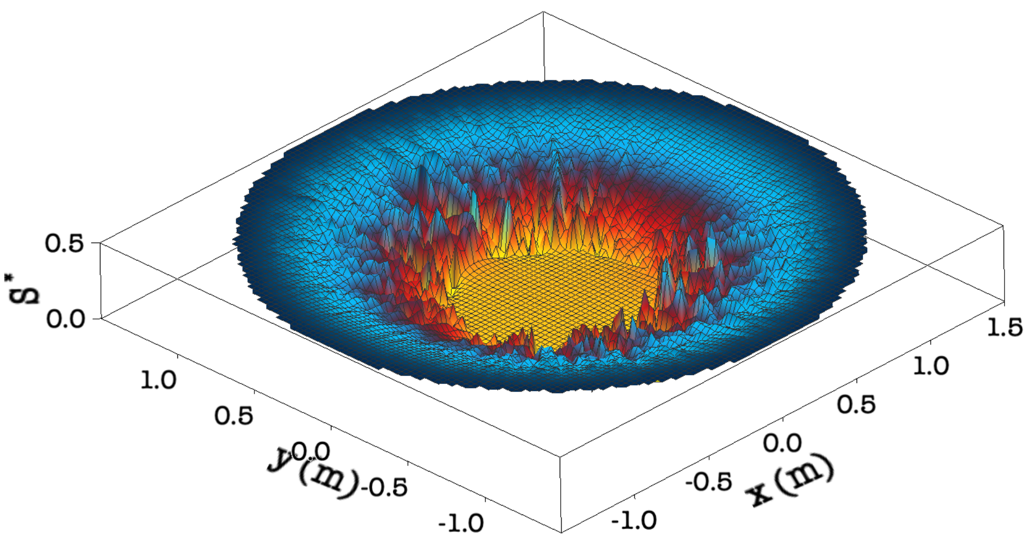

Fig.14 Analysis results for an anisotropic distribution of the degree of saturation.

parameters. The validity of the exact solution was confirmed using the specified water diffusion coefficient, which was compared with the change in the water content in the drying deformation test. Furthermore, using the verified exact solution, we proposed a new stochastic differential equation that can be used to express the change in the water content in an EDZ. In this equation, the hydraulic conductivity of the EDZ is expressed using nondifferentiable Brownian motion. We confirmed the validity of our proposed stochastic differential equation using calculations that assume a sedimentary rock tunnel, thus verifying the properties of the water content in an EDZ can be appropriately expressed. Using the proposed 1D stochastic differential equation, we demonstrated that the water content distribution in the EDZ around a 2D tunnel can also be evaluated.

Acknowledgement

This study was partially supported by a grant from the Ministry of Economy, Trade, and Industry, Japan.

References

1. Abdoul, R.G., Omidvar, M., Barari, A., 2011. Infiltration in unsaturated soils – An analytical approach. Comput Geotech. 38, 777-782.
2. ASTM, 2004. Standard test method for determination of pore volume and pore volume distribution of soil and rock by mercury intrusion porosimetry. ASTM d4404-84.
3. Autio, J., Siitari-Kauppi, M., Timonen, J., Hartikainen, K., Hartikainen, J., 1998. Determination of the porosity, permeability and diffusivity of rock in the excavation-disturbed zone around full-scale deposition holes using the 14c-pmma and he-gas methods. Journal of Contaminant Hydrology. 35(1-3), 19-29.
4. Barry, D., Parlange, J.Y., Sander, G., Sivaplan, M., 1993. A class of exact solutions for Richards'' equation. Journal of Hydrology. 142(1-4), 29-46.
5. Broadbridge, P., Daly, E., Goard, J., 2017. Exact solutions of the Richards' equa- tion with

nonlinear plant-root extraction. Water Resources Research. 53(11), 9679-9691.

6. Esaki, T., Zhang, M., Mitani, Y., 1996. Comparative tests for evaluating permeability changes of a compacted bentonite/sand mixture during shear. MRS Online Proceedings Library. 465, 979-986.
7. Farlow, S., 1993. Partial differential equations for scientists and engineers, Courier Corporation.
8. Farthing, M.W., Ogden, F.L., 2017. Numerical solution of Richards' equation: A review of advances and challenges. Soil Science Society of America Journal. 81(6), 1257-1269.
9. Fleming, J.F., Parlange, J., Hogarth, W., 1984. Scaling of flux and water content relations: comparison of optimal and exact results. Soil Science. 137, 464-468.
10. Gardner, W., 1958. Some steady-state solutions of the unsaturated moisture flow equation with application to evaporation from a water table. Soil Science. 85(4), 228-232.
11. Higham, D.J., 2001. An algorithmic introduction to numerical simulation of stochastic differential equations. SIAM review. 43(3), 525-546.
12. Hooshyar, M., Wang, D., 2016. An analytical solution of Richards' equation providing the physical basis of scs curve number method and its proportionality relationship. Water Resources Research. 52(8), 6611-6620.
13. Hou, Z., 2003. Mechanical and hydraulic behavior of rock salt in the excavation disturbed zone around underground facilities. Int. J. Rock Mech. Min. Sci. 40(5), 725-738.
14. Kurikami, H., Takeuchi, R., Yabuuchi, S., 2008. Scale effect and heterogeneity of hydraulic conductivity of sedimentary rocks at horonobe url site. Physics and Chemistry of the Earth, Parts A/B/C, 33, S37-S44.
15. Lisjak, A., Tatone, B.S., Mahabadi, O.K., Grasselli, G., Marschall, P., Lanyon, G.W., . . . Nussbaum, C., 2016. Hybrid finite-discrete element simulation of the edz formation and mechanical sealing process around a microtunnel in opalinus clay. Rock Mech. Rock Eng. 49(5), 1849-1873.

16. Marschall, P., Distinguin, M., Shao, H., Bossart, P., Enachescu, C., Trick, T., 2006. Creation and evolution of damage zones around a microtunnel in a claystone formation of the swiss jura mountains.. In Spe international sympo- sium and exhibition on formation damage control.
17. Osada, M., 2014. Drying-induced deformation characteristics of rocks. In Isrm international symposium-8th asian rock mechanics symposium.
18. Richards, L.A., 1931. Capillary conduction of liquids through porous mediums. Physics. 1(5), 318-333.
19. Ross, P., Parlange, J.Y., 1994. Comparing exact and numerical solutions of Richards' equation for one-dimentional infiltration and drainage. Soil Science. 157(6), 341-344.
20. Seiki, T., 2017. Introduction to oya tuff. Journal of the Society of Materials Science, Japan. 66(11), 793-798. (In Japanese)
21. Sun, W., Cui, Y., 2020. Determining the soil-water retention curve using mercury intrusion porosimetry test in consideration of soil volume change. Journal of Rock Mechanics and Geotechnical Engineering. 12 (5), 1070-1079.
22. Thomas, L.K., Katz, D.L., Tek, M.R., 1968. Threshold pressure phenomena in porous media. Society of Petroleum Engineers Journal. 8(02), 174 – 184.
23. Togashi, Y., Kikumoto, M., Tani, K., Hosoda, K., Ogawa, K., 2018. Detection of deformation anisotropy of tuff by a single triaxial test on a single specimen. Int. J. Rock Mech. Min. Sci. 108, 23-36. doi: 10.1016/j.ijrmms.2018.04.054
24. Togashi, Y., Kikumoto, M., Tani, K., Hosoda, K., Ogawa, K., 2019. Non-axisymmetric and/or non-elementary response of anisotropic tuff in axisymmetric, elementary triaxial test. In E3s web of conferences (Vol. 92, p. 02008). doi: 10.1051/e3sconf/20199202008
25. Togashi, Y., Imano, T., Osada, M., Hosoda, K., Ogawa, K., 2021a. Principal strain rotation of anisotropic tuff due to continuous water-content variation. Int. J. Rock Mech. Min. Sci. 138, 104646. doi: 10.1016/j.ijrmms.2021.104646
26. Togashi, Y., Imano, T., Osada, M., 2021b. Deformation characteristics of sedimentary

rock due to continuous changes of moisture content in wetting process. In IOP conference series: Earth and environmental science (Vol. 703, p. 012021). doi: 10.1088/1755-1315/703/1/012021

27. Togashi, Y., Imano, T., Osada, M., Hosoda, K., Ogawa, K., 2021c. Principal strain rotation of anisotropic tuff due to continuous water-content variation. Int. J. Rock Mech. Min. Sci. 147, 104889. doi: 10.1016/j.ijrmms.2021.104889

28. Tracy, F.T., 2011. Analytical and numerical solutions of Richards' equation with discussions on relative hydraulic conductivity. IntechOpen.

29. Watanabe, K., Sato, K., 1979. Experimental study on permeability in fractured rock. Proceedings of the Japanese conference on hydraulics. 23, 15-20. (In Japanese)

30. Zhou, J., Liu F., He J., 2013. On Richards' equation for water transport in unsaturated soils and porous fabrics. Comput Geotech. 54, 69-71.